Rapid Fabrication of Glass Micro and Nanostructures via Laser-assisted Hot Embossing

Helen Lee May Shian, Ismayuzri Ishak, and Mohd Zairulnizam Bin Mohd Zawawi*

Faculty of Manufacturing and Mechatronic Engineering Technology, University Malaysia Pahang, 26600 Pekan, Pahang, Malaysia
**Corresponding author's e-mail: zairulnizam@ump.edu.my*

The escalating demand for glass that exhibits various surface functions has encouraged efforts to develop more efficient and economical micro-/nano-patterning of glass substrates. We propose rapid hot embossing of glass micro-/nanostructures using an infrared transmissive mold assisted by CO_2 laser irradiation. This resistless, etch-free technique utilizes the synergy of the silicon mold's high transmittance and strong optical absorption of the glass at a 10.6-μm wavelength. Furthermore, this non-isothermal process requires preheating of the glass temperature below the glass transformation point (T_g) of the glass, eliminating the soaking time, and using a short contact pressing time and a lower pressing load to produce high-resolution space patterns. The method is capable of instantaneous high-resolution replication of various grating patterns from the nano- to microscale with a single laser scan. By controlling the scanning speed and ensuring sufficient pressure and heating depth on the glass surface, 250-nm to 50-μm line- widths and space patterns were embossed in a few seconds with excellent replication fidelity. The laser-assisted hot embossing methods developed in this study facilitated high-throughput, energy-efficient, reproducible, and highly accurate micro-/nano-patterning of glass surfaces.

DOI: 10.2961/jlmn.2023.01.2001
Keywords: laser-assisted, micro/nanostructures, hot embossing, optical glass, energy-efficient

1. Introduction

Devices are becoming ever-smaller and more compact; complex, integrated micro-/nano-surfaces that afford high accuracy and excellent performance are required. Engineered micro-/nanostructures allow the realization of many optical devices that could be potentially exploited in numerous applications such as optical communication [1-3], point-of-care testing for medical diagnostics [4], bio-inspired surfaces [5,6], and biosensors [7,8]. Polymers are most commonly employed as the base material in these structures, due to their relatively cheap price and soft processing characteristics. However, glass based micro-/nanostructures exhibit higher light transmittance, excellent thermal and chemical stability, as well as superior mechanical and wear resistance. Although many technologies can be used to pattern glass surfaces, commercialization is viable only if production efficiency is acceptable and product performance assured.

Numerous fabrication techniques have been investigated extensively to produce these micro-/nanostructures, including photolithography/e-beam lithography and etching [9,10], nano-imprint lithography [11-13], focused ion beam (FIB) machining [14], sol-gel method [15], and machining [16]. Currently, when fabricating high-aspect-ratio features in the micro-/nano-meter range, most master stamp processes feature serial microfabrication [photolithography, electron beam lithography (EBL), focused ion beam machining (FIB), and etching] depending on the required pattern resolution and shape. Unfortunately, these processes are either time-consuming or require elaborate equipment and/or a large number of processing steps. Direct patterning of micro-/nanostructures onto glass using a laser has also been reported [17-19]. However, the process is slow; multiple laser passes are required for patterning. Furthermore, most pattern sizes and shapes are periodic in nature; three-dimensional geometric patterns are difficult to create.

Hot embossing is a relatively simple and inexpensive process and, as such, is considered to be one of the most promising and efficient methods for fabricating glass micro-/nanostructures. The process does not require photoresist coating, and proceeds in a single step. After fabrication of a high-quality durable mold, mass production is relatively simple and inexpensive. The use of glassy carbon mold (GC) for glass hot embossing had been reported [20-22]. GC is a very durable mold material; GC can withstand temperatures up to 2,000°C. Also, no coating is required given the excellent anti-adhesive properties of GC. However, although GC has been used for precision molding of lens glass, fabrication of surface micro-/nanostructures on the large GC molds employed to manufacture diffractive optical components remains very challenging. The issues include the high surface roughness of the available raw material, brittleness, and incompatibility with existing micro-/nano-fabrication technology.

Despite the continuous developments with regard to imprinting high-resolution patterns directly onto the glass substrate, conventional glass hot embossing (especially of nanoscale features) remains in the prototyping stage. The hot embossing process suffers from a long thermal cycle, a poor filling ratio especially for sub-micron features, and excessive thermal deformation of the bulk glass when the imprinting temperature and pressing load are too high [23-25]. In addition, the thermal cycle (heating, soaking, pressing, annealing, and cooling) is very long. All steps are performed inside a closed molding chamber, and the total cycle time

ranges from 20 mins to 1 hour, depending on pattern size and the chemical composition of the glass. To date, it is still challenging to fabricate, efficiently, glass-based micro-/nanodevices of high quality using conventional hot embossing.

The application of an external source to supplement the hot embossing process, such as by ultrasonic, electrical, or laser-assisted means is gaining interest. For example, ultrasonic-assisted embossing of polycarbonate has been demonstrated, using a steel stamp [26]; grating patterns of 4-µm and 500-nm were embossed with an average fill rate of more than 75%. Electrostatic sources have been applied to replicate 0.3 to 5-µm line widths and space patterns, with a mold pattern height of 150-nm [27]. Laser-aided material processing has attracted a great deal of interest and has been employed in micro-/nanofabrication. Focused laser irradiation can easily create extreme temperatures; both precision and control are excellent. In the context of micro-/nanofabrication, several reports on laser-assisted patterning have appeared.

Laser-assisted hot embossing of periodic grating nanostructures and microlens arrays on polymethylmethacrylate films have also been demonstrated [28,29], as well as the replication of glass nanostructures using laser-assisted thermal imprinting [30]; however, only one type of pattern was used, and the pattern feature size was below 1-µm. Therefore, it is essential to explore the capacity of the laser-assisted method to imprint other type of nanostructures pattern including the micro scale structures. Laser-assisted embossing of microdimples on glass were produced using a diode laser as the heat source [31]; the laser beam traveled through the backside of the glass, in which the heated mold transferred the heat to the glass to copy the ball-shaped pattern. However, this particular study did not involve replication of fine-patterned structures.

Here, we report on a laser-assisted hot embossing method that enables rapid imprinting of various micro- and nanoscale grating patterns on optical glass substrates, with a shorter overall thermal cycle.

The comparison between glass temperature profiles obtained using conventional hot embossing and laser-assisted glass hot embossing is shown in Fig.1(a). Our method featured CO_2 laser-driven surface heating during the embossing step as shown in Fig. 1(c). Heat temporarily absorbed after well-controlled CO_2 laser irradiation reduced the glass surface viscosity and facilitated filling by glass of micro-/nanostructures created during embossing. In addition, this non-isothermal process requires preheating of the glass temperature below the glass T_g of the glass, eliminating the soaking time, and using a short contact pressing time and a lower pressing load to produce high-resolution space patterns. Therefore, the overall thermal cycle for one embossing cycle was significantly reduced.

In conventional hot embossing, heating, pressing, and cooling steps are performed in series inside a closed molding chamber as shown in Fig.1 (b). Even though not demonstrated in this study, we believed that the production efficacy could be further improved if the process setup was designed to be continuous. For instance, the glass samples could be readily heated externally such as in an oven or heating block and then transferred to the pressing station for replication procedure. Also, after demolding, the patterned glass could be transferred to other station for external cooling.

An infrared transmissive silicon mold with a pattern of 750-nm line width, and a 350-nm spacing (~330-nm height) and a 250-nm line width and a space (L&S) pattern (~160-nm height) were used in the experiment. In addition, a microscale grating pattern with an L&S pattern that included 5, 10, and 50-µm microstructures was also replicated on the glass substrate, in which the occurrence of glass filling into the micro-structured mold cavities was investigated. The relationship between the processing conditions and characteristics of the embossed glass pattern were analyzed using scanning electron microscope (SEM), focused ion-beam scanning electron microscope (FIB-SEM), atomic force microscope (AFM) and laser scanning confocal microscope (LSCM).

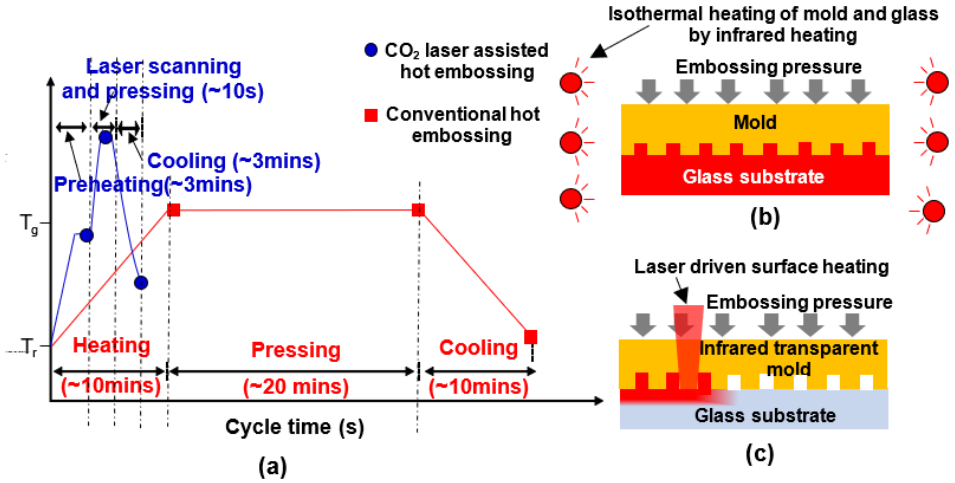

Fig. 1 (a) Comparison between glass temperature profiles obtained using conventional hot embossing and CO_2 laser-assisted glass hot embossing. T_g and T_r represent the glass transition temperature and room temperature, respectively. (b) Isothermal heating of mold and glass in conventional hot embossing, (c) laser driven surface heating in CO_2 laser-assisted glass hot embossing.

2. Materials and methods

The silicone mold used in the experiment was outsourced from Kyodo International Inc. (Kanagawa, Japan). All of the molds were coated with silicon nitride using a plasma-enhanced chemical vapor deposition process to provide anti-adhesion at the glass-silicon mold interface and to ease demolding. The mid-infrared optical transmittance of the 1000-µm-thick silicon mold at a wavelength of 10.6-µm was ~80%, as indicated by Fourier transform infrared spectroscopy measurements [3,30]. The optical glass samples used in the experiment were K-PG375 samples (Sumita Inc., Saitama, Japan); the T_g value and yield point (At) of the glass are 344°C and 367°C, respectively.

A schematic diagram of the laser scanning-assisted hot embossing setup is shown in Fig. 2. From top to bottom, the self-made press assembly consisted of a top plate, an upper insulator, a top and bottom heater block, a lower insulator and a lower plate. An infrared transmissive zinc selenide (ZnSe) block, which acted as a restraining layer, was mechanically clamped between the top plate and the silicon mold. A pair of guide pins and bush assembly were used for the purpose of alignment between the upper half and lower half press assembly. In each guide pin, a spring was inserted which act as a damper during the contact pressing. The type of laser source used was a continuous CO_2 laser, with an operating wavelength of 10.6-µm. The beam source diameter was 1.8 mm at $1/e^2$, in which the focal length could be adjusted by varying the height of the focusing lens. The raster scanning movement of the laser beam was controlled by a scanning galvanometer.

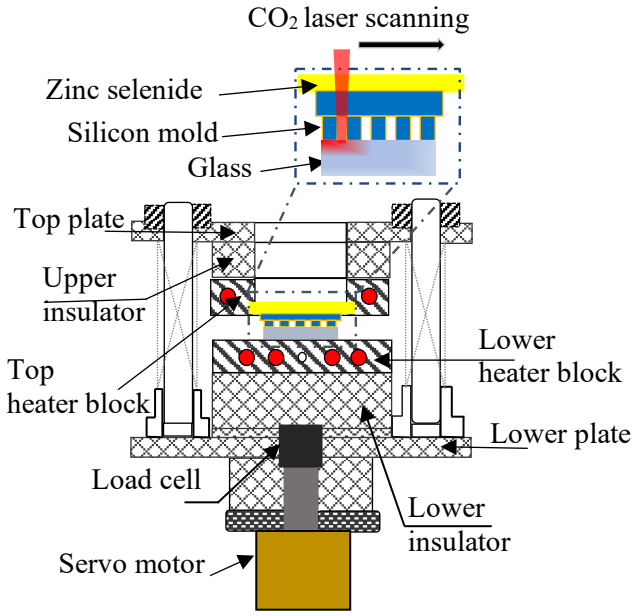

Fig. 2 Schematics of the laser assisted hot embossing setup.

Once the preheated glass was sandwiched between the silicon mold and the lower heater block under load, the sample was irradiated with a CO_2 laser, in which the beam passed through both the infrared transmissive ZnSe block and the silicon mold. The absorbed photon energy of the glass provided substantial heating of the glass surfaces, thus reducing the viscosity of the glass surface and accelerating the filling of the glass material in the micro/nanostructure mold cavities.

3. Result and discussions

Based on the thermal properties given by Sumita Inc., the glass transition temperature (T_g) and coefficient of thermal expansion for the K-PG375 optical glass are 344°C and 160 x 10^{-7}°C^{-1} respectively. For similar glass material, the recommended imprinting temperature ranges from 360°C to 380°C, according to the literature [32-34]. However, when used in conjunction with a laser-assisted method, as demonstrated in the current study, we found that this temperature range was too high, resulting in excessive bulk glass deformation with poor pattern transfer. Therefore, the glass was heated slightly below the T_g of the glass. We confirmed that the suitable preheating temperature was in the range of 320°C to 335°C. When the preheating temperature was below 320°C, the glass surface was either not imprinted or cracked, depending on the laser irradiation conditions used. For preheating temperatures above 335°C, the glass tended to show excessive deformation and thickness reduction, which at the same time also degraded the quality of the imprinted pattern. It is worth mentioning again that our proposed method is a non-isothermal process. Therefore, since the glass preheating temperature was below the glass T_g, excessive pressing load must be avoided. With respect to the imprinting load, we confirmed that a moderate load in the range of 0.2 to 0.5 MPa was sufficient to ensure good replication quality, which was substantially low compared to the conventional hot embossing demonstrated in the previous work using a similar glass material [32-34]. After each laser scan, only a thin layer on the glass surface was rapidly raised above the glass T_g, the majority glass bulk glass temperature remains below the glass T_g. This provides a more efficient flow of the viscous glass material onto the patterned mold cavities, minimizing the effect of glass lateral deformation; which normally occurred during the conventional hot embossing.

Heat accumulation effect during the continuous laser scanning procedure could not be neglected. Trade-offs between mold durability, embossed pattern quality and cycle time need to be considered. Therefore, suitable combination of the laser power and spot size, scanning speed, scanning path style and beam scanning overlap ratio are necessary. The smallest beam spot size that could be obtained in our system was about 0.15 mm. However, we chose a larger beam diameter (1.5 ± 0.5 mm) during the laser scanning procedure, to prevent the formation of microcracks in the glass surface. We noticed that the combination of spiral laser path (either rectangular or circular) and focused laser spot size resulted in excessive temperature rise on the glass surface during the scanning procedure. However, we did not observe any adhesion of the glass to the mold or damaged glass pattern when the combination of raster scanning path style, laser spot size

of about 1.5±0.5 mm, laser scanning speed of above 5mm/s and beam scanning overlap ratio of about 0.3 mm was employed throughout all the experiments.

Visible bright diffraction on the glass surface after laser scanning is an indicator of pattern transfer, which occurred when the scanning speed varied between 5 and 25 mm/s. At a scanning speed of 30 mm/s, the replication failed due to the insufficient temperature rise at the glass surface, i.e., the laser interaction time was too short. When the scanning speed was reduced to 1 mm/s, we experienced several problems such as excessive deformation in the bulk glass and strong stiction of the glass to the mold after demolding or glass cracking. The left Fig. 3(a) shows a photograph of embossed glass with four brightly diffracted colored lines after four passes of the CO_2 laser without overlapping of the beam source diameter. The region outside the irradiation area was not embossed, because the initial glass temperature (320°C) was below the T_g (344°C). In terms of replication quality, so far, we did not notice any differences when the scanning path was performed either horizontally or perpendicularly to the grating direction.

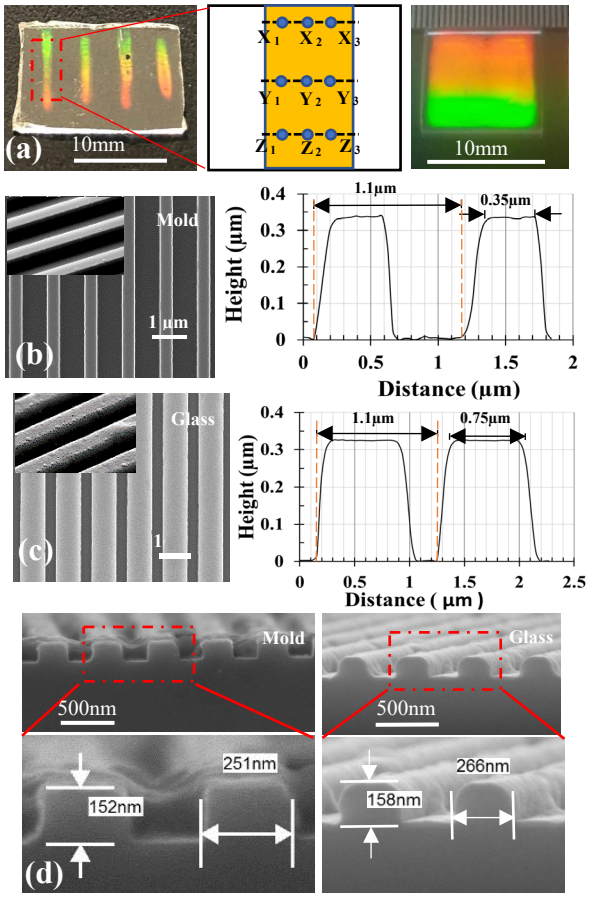

Fig. 3 (a) Photograph of embossed glass with four brightly diffracted colored lines after four passes of the CO_2 laser without overlapping of the beam scanning (left), points at which an atomic force microscope (AFM) was used to measure imprinted pattern heights within the region after single laser scan (middle) and photograph of a 100-mm^2 area of embossed glass after completion of laser scanning; combinations of scanning paths are shown with an overlap in the beam source diameter of 0.3 mm (right), (b-c) SEM image (left) and AFM 2D profile (right) of the 350-nm line width and 750-nm space silicon molds and corresponding embossed glass, (d) SEM cross-sectional image of 250-nm L/S silicon mold (left) and embossed glass (right) and its enlargement view.

It was extremely difficult to obtain a perfectly uniform heat distribution on the glass surface during the laser scanning due to several factors. We clearly observed that the use of different glass sample sizes also gave different diffracted colored lines width. The effect of gaussian beam distribution may also contribute, where the intensity profile at any beam radius varies and not constant. Also, due to the inertia of the galvanometer mirrors used in the experiment; it also very difficult to obtain a constant laser beam focal length as well as uniform heat distribution along the laser scanning path. In addition, as the mirror deflecting the beam during the scanning, the shape of the beam source diameter itself, the energy density and the location of the beam might be different. However, these discrepancies can be compensated by appropriately overlapping the beam source diameter during the scanning procedure.

We explore the laser processing parameters by observing the visible bright diffraction on the glass surface after each single laser scan. Within the bright diffracted region inside the laser path, we measured the embossed pattern height using AFM. The embossed pattern height was randomly measured in three locations perpendicular to the straight-line pass using an AFM as shown in the middle of Fig.3(a). The embossed heights were (~330 ± 15-nm) at a laser line width of approximately 1 mm (Table 1). These measurements are important for us to verify the region that conform to high replication quality after each single laser scan. Based on these AFM measurements, the distance between the scanning line (beam scanning overlap ratio) was decided so that no seam was visible after complete scanning procedure.

The right Fig. 3(a) shows a photograph of a 100-mm^2 area of embossed glass after completion of laser scanning; combinations of scanning paths are shown with an overlap in the beam source diameter of 0.3 mm. Fig. 3(b) and Fig. 3(c) show SEM images and AFM profiles of the silicon mold and the embossed glass; the feature was composed of a 750-nm line width, a 350-nm spacing, a 1100-nm pitch and a ~331-nm height. The embossed glass pattern was consistent with the silicon mold with an inverse shape having pattern feature of 750-nm line width, a 350-nm spacing, a 1100-nm pitch and a ~ 324-nm height. In this experiment, a 100-mm^2

Table 1 Embossed glass pattern heights after single laser scan, based on AFM measurements

Point	Height (nm)	Point	Height (nm)	Point	Height (nm)
X_1	322	Y_1	331	Z_1	320
X_2	325	Y_2	330	Z_2	315
X_3	320	Y_3	321	Z_3	326

glass area was imprinted using a laser power of 30 W, a beam source diameter of approximately 1.0 mm, a scanning speed of 15 mm/s, scanning process time of about 9s and an embossing pressure of 0.3 MPa. The glass had been successfully separated from the mold without cohesion, and the embossed grating pattern results showed high replication fidelity, without any structural damage or cracking in the bulk glass. We believed several conditions such as glass shrinkage after the laser assisted scanning procedure promote the demolding process. The coefficient of thermal expansion of the silicon mold and K-PG375 glass are 30 x 10^{-7}°C^{-1} and 160 x 10^{-7}°C^{-1} respectively. Therefore, it is reasonable to say that the glass will shrink more than the silicon mold during cooling. Furthermore, the wall of the patterned silicon molds is slightly tapered as well as having a low aspect ratio pattern. Furthermore, the silicon nitride coating also provides anti-adhesion at the glass interface. The tilted SEM [inset Fig. 3] and AFM two-dimensional (2D) images further confirmed that the glass had been imprinted successfully and demolded. Also, the flat rectangular cross-sectional profile of the embossed nanograting indicated that the glass material had reached the bottom of the silicon mold grating pattern.

Up to this stage, the short contact embossing time demonstrated was evidence of the CO_2 laser-driven surface heating effect, which cannot be obtained using the conventional embossing method. Using similar processing conditions, we also embossed a narrower nanograting pattern, a 250-nm L&S pattern (height: ~160-nm). Due to the AFM measurement error artifact, we confirmed the quality of the imprinted glass using SEM cross-sectional view, as shown in Fig. 3(d). The imprinted glass exhibited good replication fidelity, in which the embossed glass pattern heights were nearly identical to the mold pattern height. Furthermore, the pattern profile and dimensions were also consistent with the characteristics of the silicon mold, with a slight deviation at either end of the top corner. We measured the arithmetic average surface roughness (Ra), randomly across the patterned silicon mold and the embossed glass using AFM. Ra was confirmed by measuring the ~0.35 µm x ~0.2 µm area at five different locations, both at the top and bottom of the nanograting surface. The measured R_a of the silicon mold and embossed glass were about 3.5-nm and 2.5-nm respectively, thus a good criterion for optics applications.

It was difficult to distinguish the different processing conditions for successful replication of the two types of periodic nanograting patterns attempted in this study; this suggests less dependency of the feature size when using the proposed technique. To achieve complete pattern transfer in conventional glass hot embossing, the selection of the optimized imprinting process parameters, mainly the temperature, pressure, and holding time, are highly dependent on the feature pattern size that includes the line width, duty ratio, and aspect ratio [23-25]. This also suggests the possibility of using this method to imprint smaller nanoscale patterns as well as higher aspect ratio pattern features. In our experiment, we used low power CO_2 laser source (30W). In the market, more powerful lasers; up to several kilowatts are available. We believed that with the application of high laser power facility, this approach could also be used for patterning other glass materials such as fused silica, soda lime and other low T_g glass.

We explored further the capability of our proposed method to replicate microscale grating patterns (L&S patterns of 5, 10, and 50-µm in size). The average depth of all of the grating patterns was about 5.5-µm. The glass was imprinted using a laser scanning speed of 5 mm/s, a beam source diameter of 2.0 mm, a scanning beam overlap ratio of 20% (0.4 mm), a preheating temperature of 330°C, and an imprinting load of 0.4 MPa. The total cycle time for the scanning procedure was about 10 s for each sample. The laser scanning confocal microscope (LSCM) measurement (a 3D image and 2D-cross-sectional profile) of the silicon mold and the corresponding imprinted glass are shown in Fig. 4.

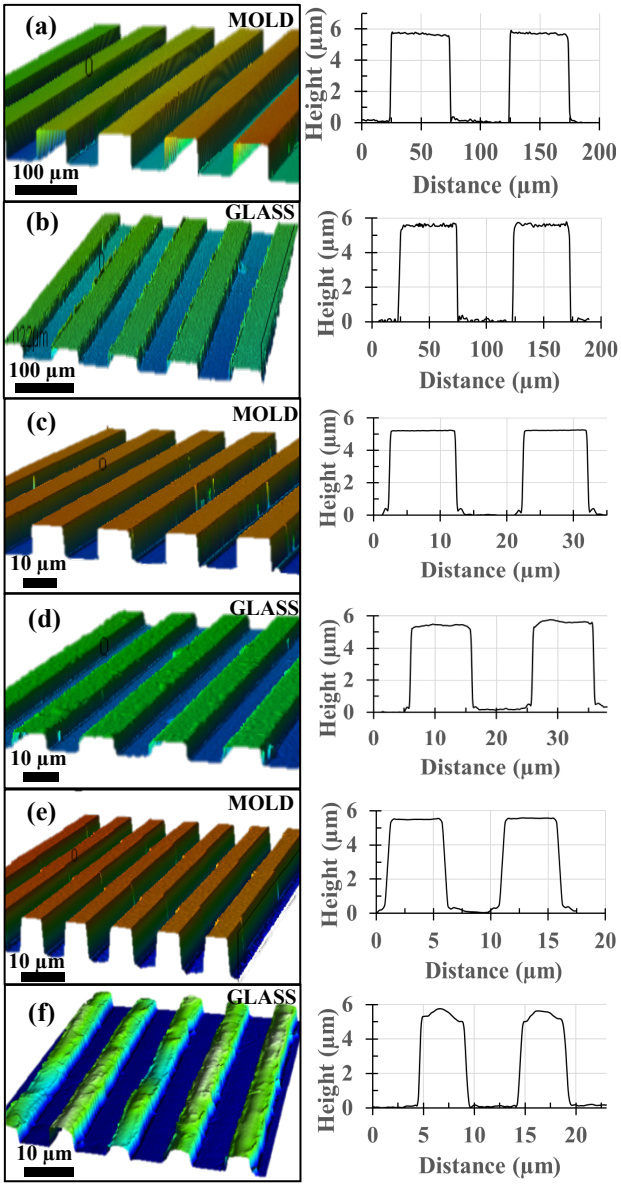

Fig. 4 LSCM 3D profile (left) and LSCM 2D cross-section (right) of silicon mold and embossed glass produced by laser-assisted scanning process (a-b) 50-µm L/S, (c-d) 10-µm L/S and (e-f) 5-µm L/S.

Clearly, for the 50- and 10-µm grating patterns, the glass had been imprinted successfully. Evidence of a flat smooth-top rectangular-shaped pattern was visible for both grating patterns. This suggests that a complete replication height had

been obtained. Meanwhile, for the 5-µm grating pattern, although the shape of the imprinted grating pattern was slightly rounded at the grating corner, the replication height at the top center of the grating was close to the mold height. This was expected because, for a smaller grating pattern, the deformation resistance of the glass material into the microstructure mold cavities increases, especially for patterns with a higher aspect ratio. We believe that with slight optimization, such as a reduction in the scanning speed and an increase in the imprinting load, that the replication fidelity can be improved. Overall, the embossed glass profile result presented above demonstrates that complete glass replication height can be achieved under optimized processing conditions.

The relationship between the embossed glass filling ratio and the laser scanning speed in the replication of microscale grating patterns of 5, 10, and 50-µm is shown in Fig. 5; the filling ratio improved as the scanning speed decreased. A sufficient scanning speed ensures a temperature rise well above the glass T_g at the glass surface, while at the same time reducing the viscosity of the glass surface. This permits easier squeeze flow of the glass material into the mold cavities. The glass flow evolved from a rounded shape to a rectangular cross-sectional shape, with a decrease in the scanning speed. With a sufficient finite amount of laser interaction time with the glass substrate, the flow of the glass material into the microstructured mold cavities also improved, until full replication height was obtained. For all of the grating patterns attempted in this study, only single-peak formation flow behavior was observed, based on the occurrence of filling profile measurements under the scanning speed range conducted in this study. In conventional hot embossing, double-peak formation has been reported, especially when the embossing temperature above the glass T_g is not sufficient [24,35].

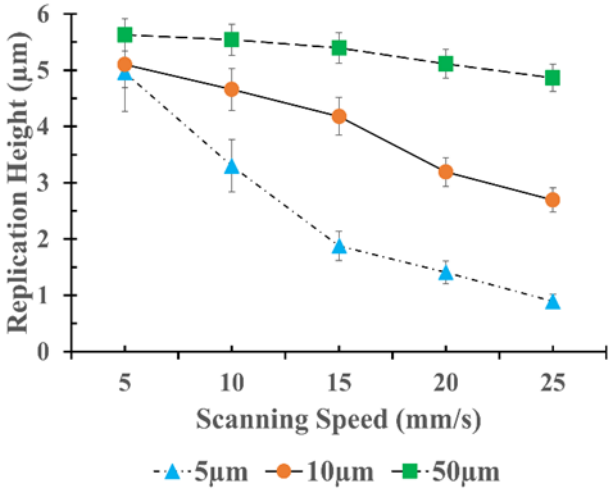

Fig. 6 Effect of aspect ratio to filling ratio of embossed glass in 5-µm, 10-µm and 50-µm size grating pattern.

The difference in the filling mode, such as single- or double-peak formation during replication, is caused by numerous factors including the viscosity of the glass, the mold pattern size, the surface tension, and the molding velocity. We speculate that the formation of only a single peak is due to the substantial thin heating at the glass surface, which significantly reduces the glass surface viscosity. Thus, the resistance of the glass flow into the mold cavities is significantly reduced either at the center or the side wall of the mold cavities. Compared to the grating period (below 1-µm), as described in the previous section, the results also indicated that the combination of a larger beam source diameter and a lower scanning speed was necessary to ensure a good filling ratio of the microscale grating pattern. This effectively ensures a sufficient heating depth, which should be larger than the mold cavity pattern height.

The effect of the grating pattern aspect ratio on the glass replication height is shown in Fig. 6. Here, the aspect ratio is defined as the ratio of the grating height to the grating width. Meanwhile the filling height percentage is express as:

$$\frac{Embossed\ glass\ pattern\ height}{Silicon\ mold\ pattern\ height} \times 100\%$$

Note that the measurement was taken after laser scanning speed of 20 mm/s. We clearly observed that, as the aspect ratio increased, the average replication height of the embossed glass decreased. For instance, the filling ratio of the 50-µm grating pattern with pattern aspect ratio of 0.1 was about 90%, which was significantly higher than the micrograting of 10-µm and 5-µm. Meanwhile, the filling ratio for the embossed glass micrograting with width of 5-µm (aspect ratio of 1) was about 26% when similar scanning speed of 20 mm/s was used. This trend is similar to what had been reported previously using the conventional approach [24,35,36]. However, in our method, replication occurred with a very short contact pressing time, instantaneously after each laser pass.

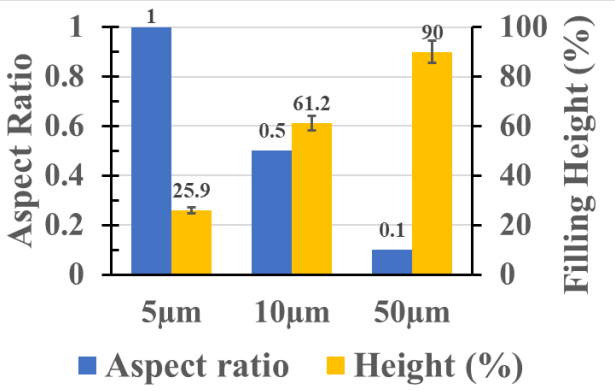

Fig. 5 Effect of scanning speed to replication height of embossed glass in 5-µm, 10-µm and 50-µm size grating pattern.

4. Conclusions

In summary, here we introduce a laser scanning-assisted hot embossing method for the fabrication of glass optics with micro-/nanoscale surface features. Our method featured CO_2 laser-driven surface heating during the embossing step. In addition, the non-isothermal process requires preheating of the glass temperature below the glass T_g of the glass, eliminating the soaking time, and using a short contact pressing

time and a lower pressing load to produce high-resolution space patterns. All the above-mentioned criteria significantly contribute to the reduction of the embossing cycle time. The method is capable of instantaneous high-resolution replication of various grating patterns from the nano- to microscale with a single laser scan. A high-resolution periodic grating pattern of different aspect ratio, ranging from 225-nm up to 50-μm, was faithfully copied to the glass surface. The pressing contact time between the mold and the glass in each molding cycle was very short, ~10 s. In addition, the overall thermal cycle was shorter and the embossing pressure was lower. Our method enables a simple, low-cost, high-throughput approach for the fabrication of fine patterns on glass.

Acknowledgments and Appendixes

This research was supported by Fundamental Research Grant Scheme, FRGS/1/2019/TK03/UMP/03/8 with the grant number RDU1901216, Ministry of Higher Education, Malaysia (MOHE).

References

[1] N.A. Baharudin, C. Fujikawa, O. Mikami, S.M. Idrus, and S. Ambran: Jpn. J. Appl. Phys., 58, (2019) SJJB02.
[2] M. Xu, Y. Xue, S. Li, L. Zhang, and H. Lu: Appl. Optics, 61, (2022) 2721.
[3] R. Han, J. Lee, B. Seong, R. Shin, D. Kim, C. Park, J. Lim, C. Joo, and S. Kang: Opt. Express, 28, (2020) 17468.
[4] Y. Xie, L. Dai, and Y. Yang: Biosens. Bioelectron.:X, 10, (2022) 100109.
[5] P. Zhou, H. Yu, Y. Zhong, W. Zou, Z. Wang, and L. Liu: Nanomicro. Lett., 12, (2020) 1.
[6] D. Wu, J. N. Wang, L.G. Niu, X. L. Zhang, S. Z. Wu, Q. D. Chen, L. P. Lee, and H. B. Sun: Adv. Opt. Mater., 2, (2014) 751.
[7] D.M. Kim, J.S. Park, S.W. Jung, J. Yeom, and S.M. Yoo: Sensors, 21, (2021) 3191.
[8] D. Wu, J. Xu, L. G. Niu, S. Z. Wu, K. Midorikawa, and K. Sugioka: Light Sci. Appl., 4, (2015) e228.
[9] M. Bu, T. Melvin, G.J. Ensell, J.S. Wilkinson, and A.G. Evans: Sens. Actuator A Phys., 115, (2004) 476.
[10] E. Yu, S.C. Kim, H.J. Lee, K.H. Oh, and M.W. Moon: Sci. Rep., 5, (2015) 9362.
[11] G. Tan, N. Inoue, T. Funabasama, M. Mita, N. Okuda, J. Mori, K. Koyama, S. Kaneko, M. Nakagawa, A. Matsuda, and M. Yoshimoto: Appl. Phys. Express, 7, (2014) 055202.
[12] Y.C. Chen, T.R. Tsai, J.P. Chu, H. Sung, J.S.C. Jang, and H. Kato: Appl. Phys. Express, 5, (2011) 012201.
[13] Y. Fan, R. Zhang, Z. Liu, D. Huang, and J. Chu: Appl. Phys. Express, 12, (2019) 095004.
[14] V. Garg, R.G. Mote, and J. Fu: Appl. Surf. Sci., 526, (2020) 146644.
[15] Y.M. Andreeva, M.M. Sergeev, R.A Zakoldaev, U.E. Gabysheva, V.P. Veiko, E.B. Yakovlev, S.I. Kudryashov, P.A. Danilov, A.A. Ionin, F. Vocanson, T.E. Itina, T.V. Antropova, and O.S. Medvedev: J. Laser Micro Nanoeng., 13, (2018) 193.
[16] E. Bordatchev and S. Nikumb: J. Laser Micro Nanoeng., 3, (2008) 175.
[17] S. Ahsan and M.S Lee: J. Laser Micro Nanoeng., 7, (2012) 202.
[18] A.I. Aguilar-Morales, S. Alamri, T. Kunze, and A.F. Lasagni: Opt. Laser. Technol., 107, (2018) 216.
[19] Z. Luo, C. Wang, K. Yin, X. Dong, D. Chu, and J.A. Duan: Appl. Phys. A., 122, (2016) 1.
[20] C. Wang, H. Huang, Y. Qian, Z. Zhang, and J. Yan: J. Manuf. Process, 62 (2021) 108.
[21] S.W, Youn, M. Takahashi, H. Goto, and R. Maeda: J. Mater. Process Tech., 187, (2007) 326.
[22] S.F. Tseng, M.F. Chen, W.T. Hsiao, C.Y. Huang, C.H. Yang, and Y.S. Chen: Opt. Lasers Eng., 57, (2014) 58.
[23] X.H. Liu, K.S. Li, J. Shen, and F. Gong: Ceram Int., 47, (2021) 18367.
[24] K.S. Li, G. Xu, X.H. Liu, and F. Gong: ACS Appl. Mater. Interfaces, 12, (2020) 36311.
[25] M. Hu, J. Xie, W. Li, and Y. Niu: Micromachines, 11, (2020) 984.
[26] Y.Y. Zhu, S. Bengsch, L. Zheng, Y.Y. Long, B.W. Roth, M.C. Wurz, J. Twiefel, and J. Wallaschek: Polymers, 13, (2021) 2417.
[27] H. Takagi, S.-i. Miyazawa, M. Takahashi, and R. Maeda: Appl. Phys. Express, 1, (2008) 024003.
[28] K. Nagato, K. Takahashi, T. Sato, J. Choi, T. Hamaguchi, and M. Nakao: J. Mater. Process Tech., 214, (2014) 2444.
[29] K. Nagato, Y. Yajima, and M. Nakao: Materials, 12, (2019) 675.
[30] M.Z. Bin Mohd Zawawi, T. Kim, M. Jung, J. Im, and S. Kang: J. Manuf. Sci. Eng., 140, (2018) 121005.
[31] T. Kurita, I. Ogura, and K. Ashida: J. Mater. Process Tech., 254, (2018) 248.
[32] Y. Saotome, K. Imai, and N. Sawanobori: J. Mater. Process Technol., 140, (2003) 379.
[33] T. Zhou, J. Yan, Z. Liang, X. Wang, R. Kobayashi, and T. Kuriyagawa: Precis. Eng, 39, (2015) 25.
[34] Y.M. Hung, Y.J. Lu, and C.K. Sung: Microelectron. Eng., 86, (2009) 577.
[35] K. Li, F. Sun, Z. Wang, and F. Gong: Opt. Eng., 61, (2022) 035107.
[36] K. Li, G. Xu, H. Luo, X. Liu, and F. Gong: Ceram Int., 46, (2020) 21517.

(Received: September 20, 2022, Accepted: January 10, 2023)